ACS OMEGA

http://pubs.acs.org/journal/acsodf

Article

Cu/ZnV_2O_4 Heterojunction Interface Promoted Methanol and Ethanol Generation from CO_2 and H_2O under UV−Vis Light Irradiation

Huihui Du, Qingxiang Ma, Xinhua Gao, and Tian-Sheng Zhao*

Cite This: *ACS Omega* 2022, 7, 7278−7286

Read Online

ACCESS | Metrics & More | Article Recommendations | Supporting Information

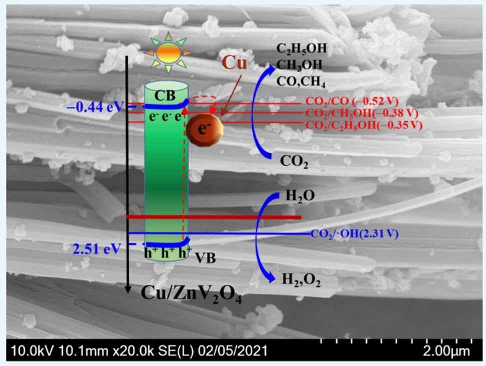

ABSTRACT: Adopting the concurrent reduction of Cu_2O during hydrothermal preparation of ZnV_2O_4, metal−semiconductor heterojunction Cu/ZnV_2O_4 nanorods were synthesized and applied to the catalytic generation of methanol and ethanol from CO_2 aerated water under UV−vis light irradiation. 10Cu/ZnV_2O_4 obtained from 10 wt % composite amount of Cu_2O exhibited a total carbon yield of 6.49 $\mu mol \cdot g^{-1} \cdot h^{-1}$. The yield of CH_3OH and C_2H_5OH reached 3.30 and 0.86 $\mu mol \cdot g^{-1} \cdot h^{-1}$, respectively. 2.5Cu/$ZnV_2O_4$ displayed the highest ethanol yield of 1.58 $\mu mol \cdot g^{-1} \cdot h^{-1}$ due to the strong absorption in the visible light. Cu/ZnV_2O_4 was characterized using X-ray diffraction (XRD), scanning transmission electron microscopy (STEM), X-ray photoelectron spectroscopy (XPS), ultraviolet−visible (UV−vis) spectra, photoluminescence (PL) spectra, transient photocurrent response, and electrochemical impedance spectroscopy (EIS). Results showed that composite Cu^0-ZnV_2O_4 increased the surface area and tuned the energy band position, which matches the reaction potential toward methanol and ethanol. The photocatalytic activity toward CH_3OH and C_2H_5OH on Cu/ZnV_2O_4 is attributed to faster transmission and a slow recombination rate of photogenerated carriers at the heterojunction interface. Multielectron reactions for the production of CH_3OH and C_2H_5OH are promoted. Free radical capture experiments indicated that the active species boost the reaction in the order of $^\bullet OH > e^- > h^+$.

■ INTRODUCTION

Photocatalytic transformation of CO_2 and H_2O to methanol and ethanol is a desired reaction. On the one hand, the excessive emissions of atherogenic CO_2 urgently need reduction/circulation to curb the greenhouse effect. On the other hand, methanol can be a viable energy carrier[1] powering the future with liquid sunshine.[2]

However, quantum yield and product selectivity in the photocatalytic reduction of CO_2 remain challenging. To harvest as much sunlight as possible and slow down recombination of photogenerated carriers, several strategies for catalyst construction have been developed, for instance, crystal-facet engineering,[3] cocatalyst modification,[4] and heterostructure engineering.[5−7] It has been recognized that the interfacial effect among semiconductors and cocatalysts can accelerate the carrier separation.[8]

Due to suitable band structure and availability, zinc vanadate has been employed in photodegradation,[9,10] batteries,[11,12] and CO_2 reduction.[13] ZnV_2O_6/g-C_3N_4 heterojunction with a 2D/2D interface increased CH_3OH formation[13] due to g-C_3N_4 being used as a mediator. ZnV_2O_7 as the hole reaction site in TiO_2/vanadate suppressed the recombination and increased the catalytic activity toward CH_4.[14]

Spinel ZnV_2O_4, an n-type semiconductor, is composed of a ZnO_4 tetrahedron and a VO_6 octahedron. 3D VO_2/ZnV_2O_4 with favorable morphology and hierarchical pores promoted photogeneration of CH_3OH, as well as CO and CH_4 from CO_2 and H_2O, in the gas−solid reaction condition, due to efficient separation of carriers.[15] Nonetheless, the preparation process of ZnV_2O_4 is difficult to control because of the multiple oxidations of VO_3^-, and the VO_x or ZnO impurity is easily formed.

As far as the metal cocatalysts are concerned, copper was reported to be active for photoreduction formation of CH_3OH from CO_2 and H_2O.[16] The valence state of the Cu active site has been studied. A study reported that Cu^{1+} is active in enhancing a multielectron photoreaction.[17] The Cu_2O (110) crystal plane enabled CO_2 to be converted to $^\bullet CO_2$, which increases the photoreduction efficiency, whereas the Cu_2O (100) plane was inert.[18] Supported Cu_2O promoted photoinduction efficiency under visible light.[19−22] Cu-modified TiO_2 exhibited light olefin selectivity of 60.4% at 150 °C, attributed to the Cu^+ species for C−C coupling.[23] Another study found

Received: December 16, 2021
Accepted: February 10, 2022
Published: February 21, 2022

https://doi.org/10.1021/acsomega.1c07108
ACS Omega 2022, 7, 7278−7286

that there exists a synergistic effect between Cu^{1+} and Cu^{2+}. Z-scheme $Na_2Ti_6O_{13}/CuO/Cu_2O$ with more Cu_2O favored H_2 evolution, whereas that with more CuO favored CH_2O and CH_3OH formation due to the coupled band gaps.[24] Furthermore, the synergy between the outside Cu and the inside Cu^+ in $Cu/Cu^+@TiO_2$ enriched electrons for CO_2 reduction to CO and CH_4.[25] Cu on TiO_2 nanosheet could activate CO_2 when Cu was oxidized.[26] Cu in Pd matrix forming Cu-Pd sites improved the CO_2 activation.[27] But excess Cu became new recombination centers of electron−holes.[28]

Although metal can enrich electrons in metal−semiconductor heterojunctions and become the active sites for CO_2 reaction,[29] the performance of Cu/ZnV_2O_4 for the catalytic generation of methanol and ethanol from an aqueous solution of CO_2 under UV−vis light irradiation has rarely been probed to our knowledge.

In this work, a two-step synthesis strategy was employed to obtain Cu/ZnV_2O_4. Cu_2O was first synthesized and then added into the hydrothermal synthesis liquid of ZnV_2O_4. The Cu^0 was obtained by the reduction of vanadate. Characterizations indicated that a metal−semiconductor heterojunction was formed at the Cu^0-ZnV_2O_4 interface and the as-constructed interface was active toward generating methanol and ethanol from an aqueous solution of CO_2 under UV−vis irradiation. The photocatalytic functionality was discussed.

■ RESULTS AND DISCUSSION

Photocatalytic Activity. The carbon product distribution of the photocatalytic CO_2 reaction with H_2O is shown in Table 1 and Figure 2. The products included CH_4, CO, CH_3OH, and C_2H_5OH. O_2 was detected but was not quantified. From Table 1, the total carbon (TC) yields on the composite samples were higher than those on ZnV_2O_4. $10Cu/ZnV_2O_4$ showed the highest TC and CH_3OH yields. $2.5Cu/ZnV_2O_4$ displayed the highest ethanol yield. The results indicated that Cu/ZnV_2O_4 promotes the generation of methanol and ethanol, particularly the ethanol yield with the C−C bond formation, and this promotion is affected by the Cu amount and the UV−vis light response (see Figure 8). The methanol and ethanol selectivity showed a slight decrease because of the increase in CO (Figure 1). This can be attributed to its light capture of a wider response, higher surface area, and higher conduct band position than $E^{\theta}_{(CO_2/CH_3OH)}$ and $E^{\theta}_{(CO_2/C_2H_5OH)}$. Composite Cu/ZnV_2O_4 formed a Mott−Schottky heterojunction interface, promoting photogenerated carrier separation and trapping photogenerated electrons to improve the 6e and 12e transfer reactions to obtain methanol and ethanol (see subsequent characterizations). The generation of methanol and ethanol can be facilitated by electron enrichment on the Cu surface through $CO_2^{\bullet-}$ and *CO formation, *CO polymerization, and formation of the C−C bond.[30,31] The combination of an appropriate amount of Cu with ZnV_2O_4 can capture and migrate photogenerated electrons and increase active sites. But excessive metals form new recombination centers inhibit the interfacial charge transfer and abate the activity.[28,32]

Table 1. Photocatalytic Activity on Synthesized Samples[a]

samples	yield (μmol·g^{-1}·h^{-1}) TC	CH_3OH	C_2H_5OH	$CH_3OH + C_2H_5OH$ sel. (%)
ZnV_2O_4	3.23	2.01	0.46	77.18
$1.25Cu/ZnV_2O_4$	5.08	2.20	1.31	69.09
$2.5Cu/ZnV_2O_4$	5.76	2.80	1.58	76.04
$5Cu/ZnV_2O_4$	5.81	2.78	0.69	59.72
$10Cu/ZnV_2O_4$	6.49	3.30	0.86	64.10
$20Cu/ZnV_2O_4$	3.37	2.19	0.39	76.56

[a]Testing conditions: 40 mg of catalyst, 80 °C, 0.2 MPa, and 4 h of irradiation.

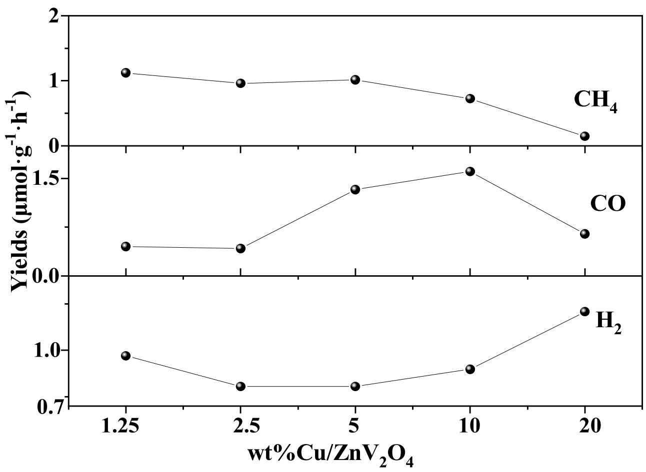

Figure 1. Gas products on Cu/ZnV_2O_4 with different Cu contents. Testing conditions: 40 mg of catalyst, 80 °C, 0.2 MPa, and 4 h of irradiation.

Figure 1 shows the gas product distribution on Cu/ZnV_2O_4 in varied composite contents of Cu_2O. As the Cu content was increased, the CH_4 yield decreased whereas the CO and H_2 yields were maximum and minimum, respectively, implying the competition of electrons between CO_2 reduction and H_2 evolution during the reaction. When the Cu content reaches 20 wt %, Cu on the surface of ZnV_2O_4 may form a new recombination center due to excessive combination. In this case, it is difficult for the multielectron reduction of CO_2 to occur. The 2e reaction dominates, and the H_2 yield increases.

The change in the alcohol yield with the irradiation time of 8 h is shown in Figure 2. The CH_3OH yield increased upon extending the irradiation time. The C_2H_5OH yield decreased

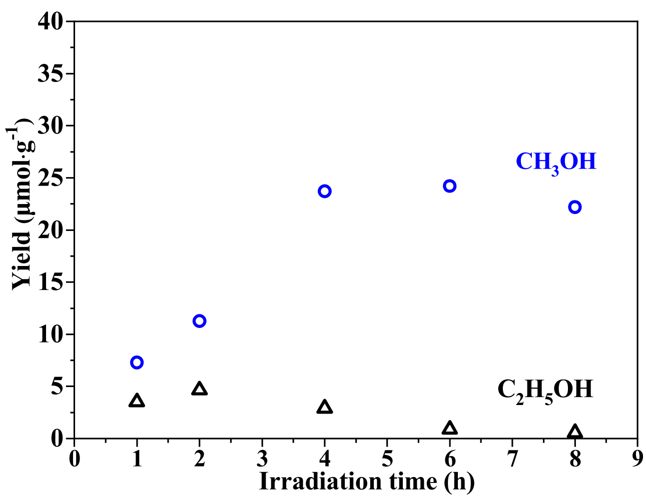

Figure 2. Change in alcohol yield with irradiation time. Testing conditions: 40 mg of $10Cu/ZnV_2O_4$, 80 °C, 0.2 MPa, and separate irradiation time.

https://doi.org/10.1021/acsomega.1c07108
ACS Omega 2022, 7, 7278−7286

after an increase. Methanol and ethanol generation became slow after 4 h at the set experimental conditions.

To understand the contribution of light, an activity test under visible light irradiation ($\lambda \geq 420$ nm) was conducted, and the result is shown in Figure S2. 10Cu/ZnV_2O_4 showed photocatalytic activity for the objective reaction under visible light irradiation, with the TC yield of 4.5 μmol·g^{-1}, indicating the response of Cu/ZnV_2O_4 to visible light. These results demonstrated that composite Cu/ZnV_2O_4 enhanced alcohol generation from CO_2 and H_2O under UV−vis irradiation.

Structure, Morphology, and Surface Area. In Figure 3, the diffraction peaks at 2θ of 18.3, 30.2, 35.7, 56.7, and 62.4°

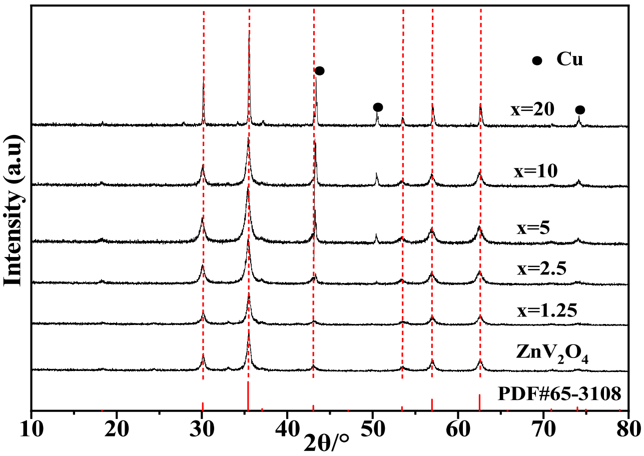

Figure 3. XRD patterns of xCu/ZnV_2O_4.

were observed, corresponding to the (111), (220), (311), (400), (422), and (440) crystal planes of ZnV_2O_4, respectively. In 2.5Cu/ZnV_2O_4, as the Cu amount was increased, Cu/ZnV_2O_4 started to produce diffraction peaks at 2θ of 43.2, 50.4, and 74.1° ascribed to (111), (200), and (220) planes of crystalline Cu, respectively (PDF# 99-0034). The intensity of Cu peaks was gradually increased. Composite metal−semiconductor Cu/ZnV_2O_4 was obtained using a two-step procedure.

Synthesized ZnV_2O_4 emerged as well-distributed nanostrips with a diameter of ca. 150 nm and rough steplike surfaces (Figure 4a).[13] 2.5Cu/ZnV_2O_4 was shaped as uniform nanorods (Figure 4b) with Cu dots (Figure 4c), indicating that Cu disperses on the surface of ZnV_2O_4 nanorods uniformly. The diffraction bright spots in the SAED photographs (Figure 4d) revealed the composite polycrystalline structure. The *d*-spacings of ca. 0.21 and 0.48 nm were ascribed to the (400) and (111) planes of ZnV_2O_4,[12] respectively. The *d*-spacing of ca. 0.22 nm was ascribed to the Cu (004) plane.[30] The heterojunction interface in Cu-ZnV_2O_4 was constructed successfully.

The high-angle annular dark-field (HAADF) TEM photographs and the EDX mapping in Figure 5 further exhibited the nanorod morphology of 2.5Cu/ZnV_2O_4 and the Zn, O, V, and Cu distribution.

Synthesized samples presented N_2 adsorption−desorption isotherms of type IV (Figure 6). From $P/P_0 > 0.8$, the adsorption volume increased due to the capillary coalescence and the appearance of the hysteresis loop of H3-type, indicating the mesopores of 2−20 nm (Figure 6, inset). The surface area and pore volume of 10Cu/ZnV_2O_4 increased by 2.39 and 1.73 times compared to those of ZnV_2O_4, respectively.

Optical Properties. The surface elemental composition and valence state of 2.5Cu/ZnV_2O_4 were analyzed using XPS. The full spectrum revealed the electron binding energy (B.E.) of Zn 2p, O 1s, and V 2p (Figure S3). As shown in Figure 7a, the B.E. peaks at 933.27 and 932.2 eV are attributed to $2p_{3/2}$ of Cu^0 and Cu^{1+}, respectively (due to part oxidation in air).[33,34] The four B.E. peaks of 523.96 and 522.80 eV and 516.80 and 515.70 eV in Figure 7b are attributed to V $2p_{1/2}$ and V $2p_{3/2}$,

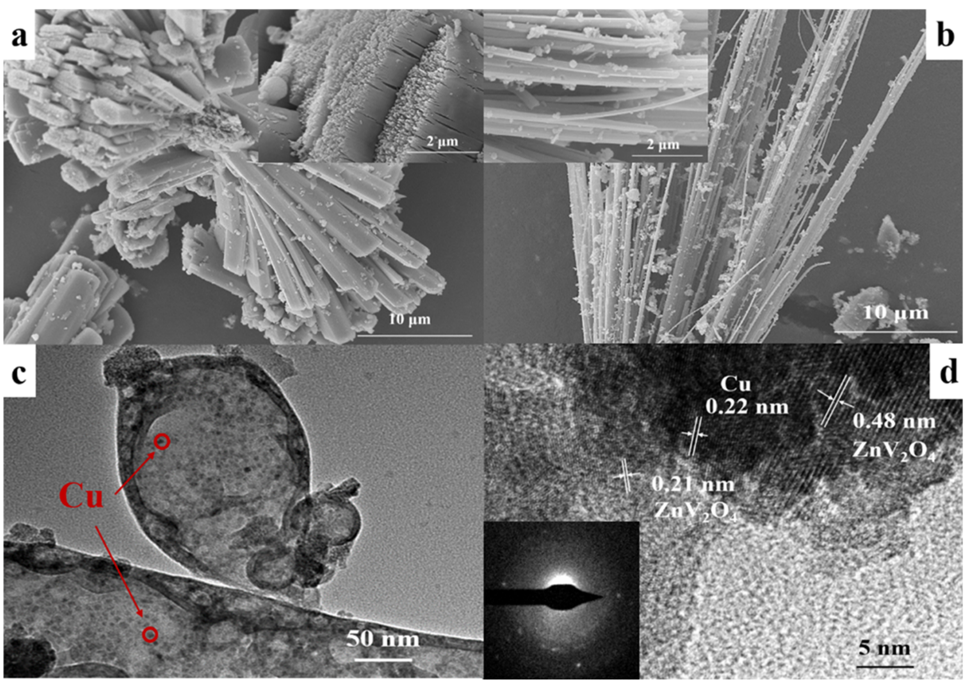

Figure 4. Scanning electron microscopy (SEM) and TEM photographs of synthesized samples (a) ZnV_2O_4 and (b−d) 2.5Cu/ZnV_2O_4.

https://doi.org/10.1021/acsomega.1c07108
ACS Omega 2022, 7, 7278−7286

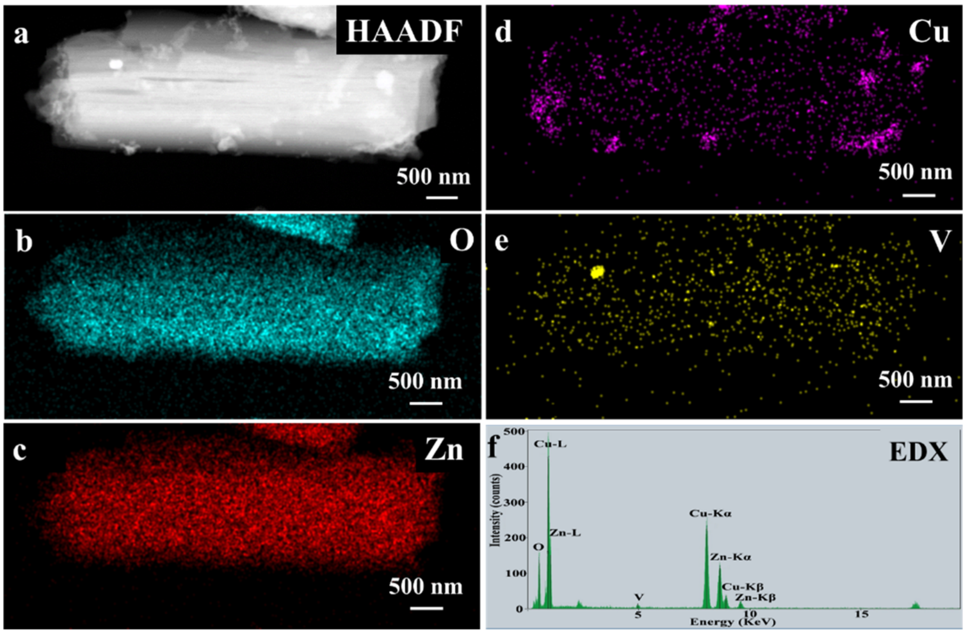

Figure 5. TEM photographs and elemental distribution for 2.5Cu/ZnV_2O_4: (a) HAADF image, (b−e) EDX mapping, and (f) EDX spectrum of 2.5Cu/ZnV_2O_4.

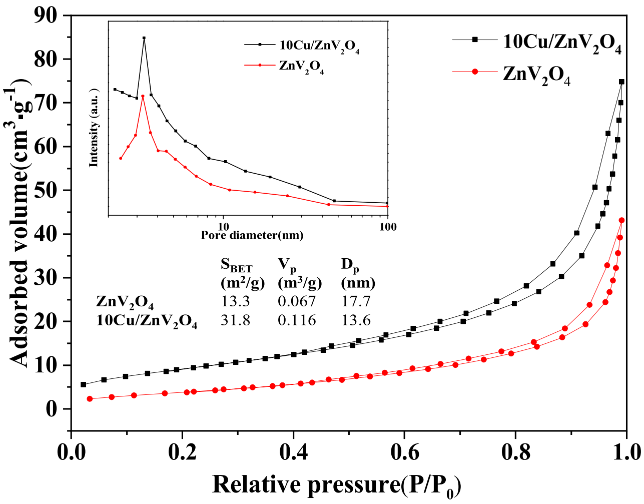

Figure 6. N_2 adsorption−desorption isotherms of synthesized samples.

respectively. The B.E. peaks of V $2p_{3/2}$ at 516.80 and 515.70 eV are ascribed to V^{5+} and V^{3+}, respectively,[9,12] indicating that the mixed state of V^{5+} and V^{3+} exists.[35,36] The B.E. peaks at 1044.98 and 1021.89 eV are attributed to Zn $2p_{1/2}$ and Zn $2p_{3/2}$, respectively, with a spin−orbit coupling of 23.15 eV, demonstrating that Zn exists as Zn^{2+} in the Cu/ZnV_2O_4 heterostructure; 531.83 and 529.67 eV are attributed to O 1s of O^{2-}, corresponding to the adsorbed oxygen and lattice oxygen, respectively. Compared with ZnV_2O_4, the B.E. of Zn, V, and O in 2.5Cu/ZnV_2O_4 exhibited a slight shift suggesting strong interaction between Cu and ZnV_2O_4 and different coordination environments associated with the changed Fermi energy level and orbital electron energy.[37]

The diffuse reflectance UV−vis absorption spectra of synthesized samples are shown in Figure 8. Strong absorption in the visible region (>420 nm) was observed. No drop absorption edge from about 700 nm was found for ZnV_2O_4. Cu/ZnV_2O_4 showed evidently an absorption edge from about 700 nm ascribed to the Schottky effect. The Mott−Schottky heterojunction interface can accelerate charge transfer,

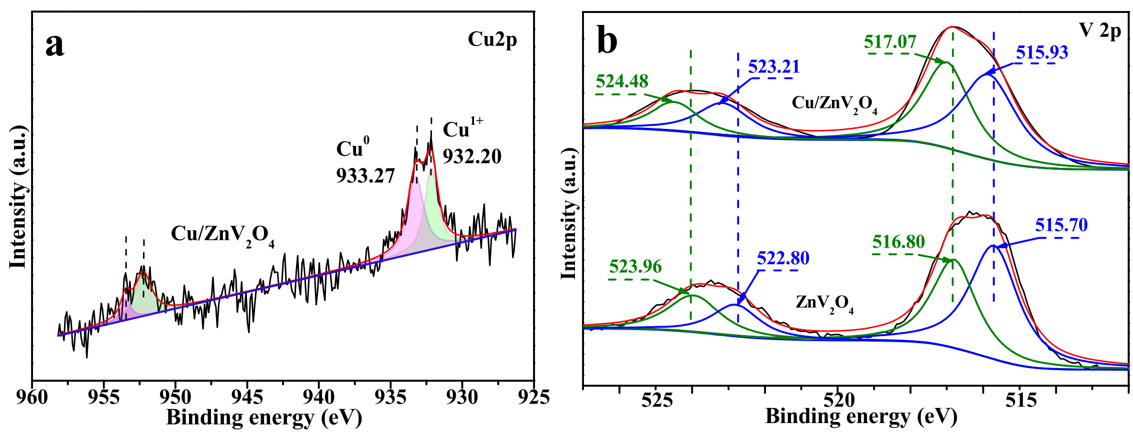

Figure 7. XPS spectra of synthesized samples (a) Cu 2p and (b) V 2p.

https://doi.org/10.1021/acsomega.1c07108
ACS Omega 2022, 7, 7278−7286

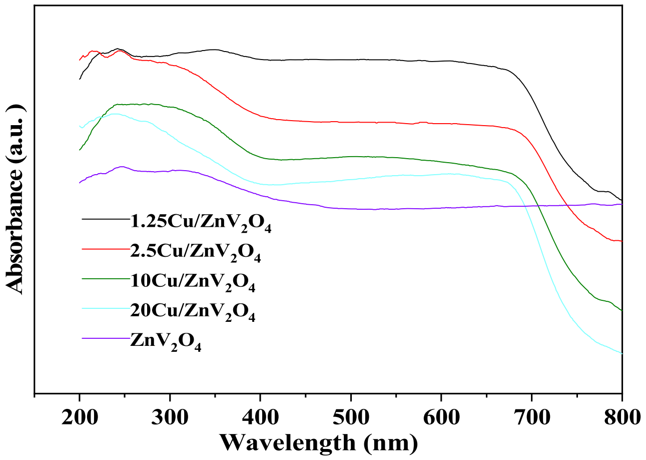

Figure 8. Diffuse reflectance UV−vis spectra of synthesized samples.

improving the catalytic activity.[29] The enhanced response of Cu/ZnV_2O_4 to visible light with an increased Cu amount is attributed to the rearrangement of the electron cloud caused by the sp hybridization at the Cu-ZnV_2O_4 heterojunction interface, which changes the Fermi energy level and narrows the apparent band gap.[24] 1.25Cu/ZnV_2O_4 and 2.5Cu/ZnV_2O_4 showed strong absorption intensity in the visible light region promoting the ethanol yield, implying that the light response is partly a factor for catalytic activity.

As shown in Figure 9, the band gap energy (E_g) for ZnV_2O_4 was 2.95 eV, similar to that reported.[37] The E_g of 2.5Cu/

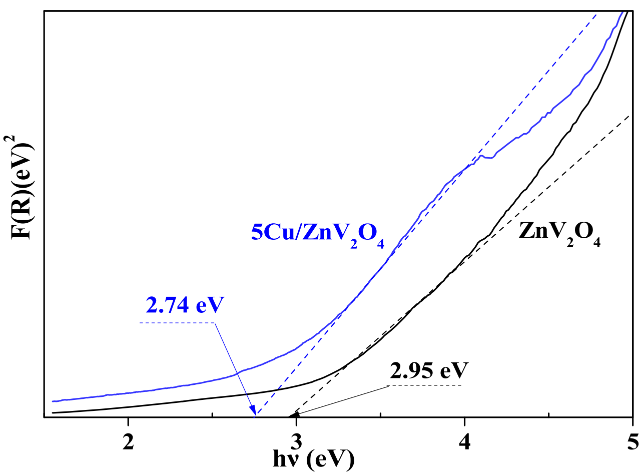

Figure 9. Fitted curves for UV−vis spectra.

ZnV_2O_4 was decreased by 0.21 eV compared with that of ZnV_2O_4, attributed to the change in the Fermi energy level of composite Cu-ZnV_2O_4.

Figure 10 shows the valence band (VB) position of ZnV_2O_4 measured by the XPS valence band spectrum.[13] The VB top position was 2.51 eV, and the conduction band (CB) bottom position was calculated as −0.44 eV from $E_g = E_{VB} - E_{CB}$.

Optoelectronic Performance. The photoluminescence (PL) spectra of synthesized samples are shown in Figure 11. ZnV_2O_4 produced PL peaks at 380, 460, and 617 nm. Compared with ZnV_2O_4, Cu/ZnV_2O_4 showed a higher PL peak intensity at around 380 nm but a lower PL peak intensity at around 460 and 617 nm. As the Cu amount was varied, the PL intensity for Cu/ZnV_2O_4 changed. The Cu amount affected

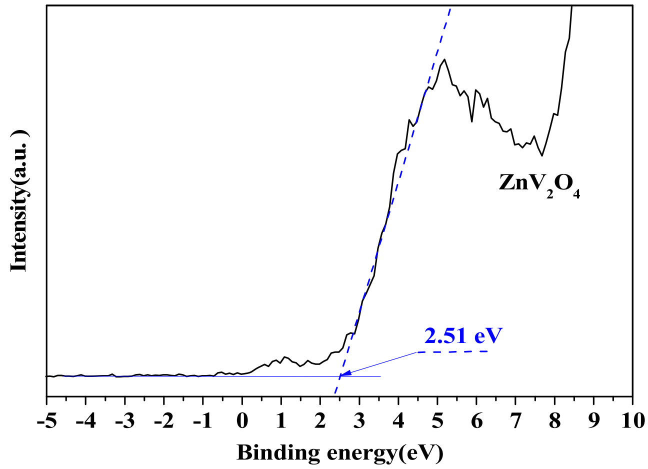

Figure 10. XPS VB spectra of ZnV_2O_4.

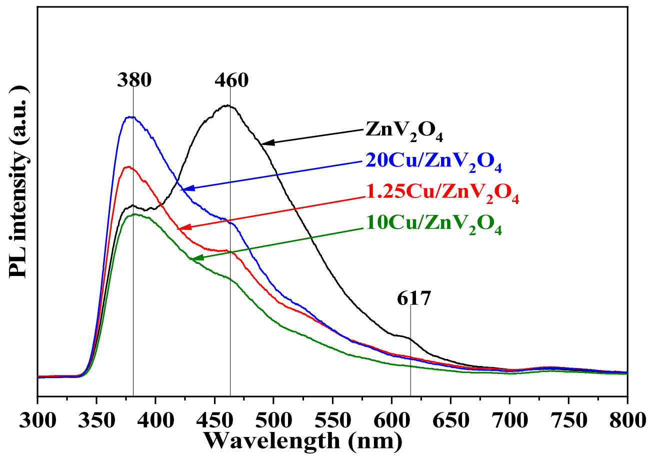

Figure 11. Photoluminescence spectra of synthesized samples.

the photoelectron transmission evidently. 10Cu/ZnV_2O_4 showed a lower PL intensity than 1.25Cu/ZnV_2O_4. The PL intensity of 20Cu/ZnV_2O_4 increased again. The PL data suggested that the recombination of photogenerated electron−holes at around 460 and 617 nm is abated due to the Cu-ZnV_2O_4 m−s heterojunction. An appropriate Cu amount benefits the photopromotion activity toward methanol and ethanol.[17,28]

The heterojunction interface separates the photogenerated electron−holes effectively and prolongs their lifetime, in accordance with the strong photocurrent response in Figure 12. No peak at 617 nm was observed for Cu/ZnV_2O_4 owing to the fast separation of photogenerated electron−holes under visible light irradiation. 10Cu/ZnV_2O_4 presented the lowest recombination rate of photogenerated electron−holes, which provides more photogenerated electrons and facilitates multi-electron reactions for methanol and ethanol generation.

Transient photocurrent response was used to characterize the photogenerated carrier density. A higher photocurrent density indicates faster migration of carriers. As shown in Figure 12, 5Cu/ZnV_2O_4 presented a current density 50 times higher than that of ZnV_2O_4, attributed to the Cu^0-ZnV_2O_4 interface, which accelerates the migration of photogenerated electrons, resulting in more photogenerated electrons. When light irradiation was turned on again, the photocurrent response increased rapidly and the photogenerated carriers

https://doi.org/10.1021/acsomega.1c07108
ACS Omega 2022, 7, 7278−7286

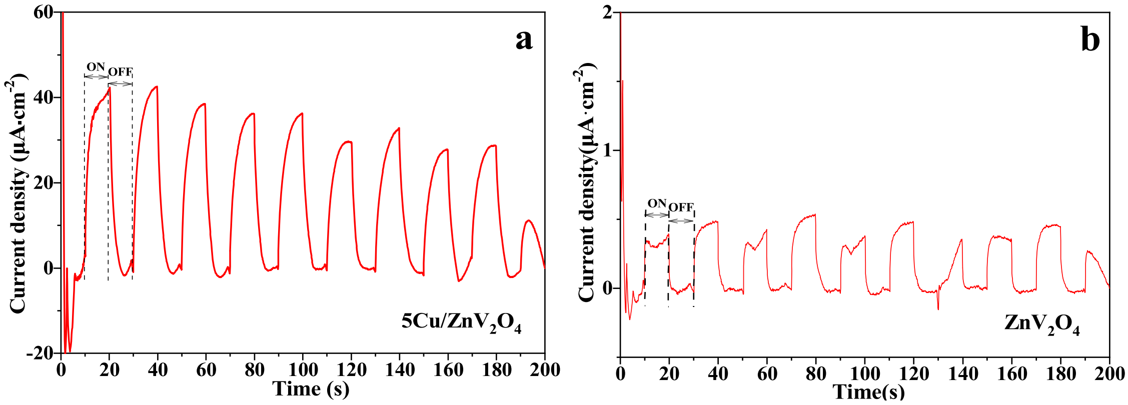

Figure 12. Transient photocurrent response curves of samples (a) 5Cu/ZnV_2O_4 and (b) ZnV_2O_4.

emerged again. The recombination rate of photogenerated carriers for Cu/ZnV_2O_4 was lower than that of ZnV_2O_4, demonstrating that composite Cu/ZnV_2O_4 can effectively suppress the recombination rate. In addition, the decrease in photocurrent density suggested the instability in the photoperformance of the catalyst.

EIS was used to characterize the resistance properties of synthesized samples. A small impedance semicircle radius stands for lower resistance to charge transfer.[38] From the Nyquist curve in Figure 13, the radius of the impedance

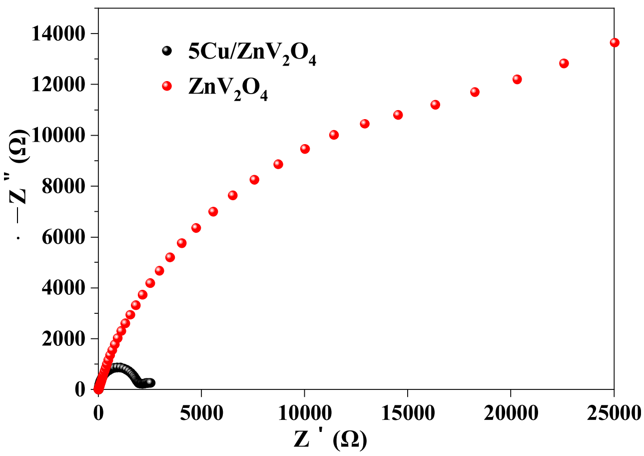

Figure 13. EIS plots of synthesized samples.

semicircle of 5Cu/ZnV_2O_4 significantly became small, suggesting that the resistance to charge transfer in the Cu-ZnV_2O_4 interface was quite low. This result confirmed that composite Cu can reduce resistance and favor charge transfer, facilitating the CO_2 reduction reaction, consistent with the activity in Table 1.

Mechanism. To understand the reaction process, free radical capture experiments were conducted for the reaction on 10Cu/ZnV_2O_4 under UV−vis light irradiation. Triethanolamine (TEOA), *tert*-butanol (TBA), and potassium dichromate ($K_2Cr_2O_7$) were added into the reaction solution to capture photogenerated holes (h^+), hydroxyl radicals (•OH), and photogenerated electrons (e^-) during the reaction,[37] respectively. From Figure 14, addition of TEOA caused an increase in CH_3OH yield by two times, implying that reduction of h^+ conduces generation of CH_3OH. No products were detected when TBA was added, indicating that •OH is

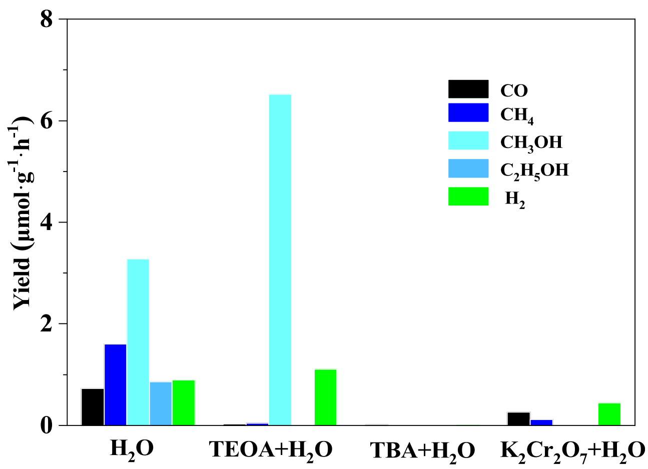

Figure 14. Free radical capture experimental conditions: 40 mg of 10Cu/ZnV_2O_4, 80 °C, 0.2 MPa, and 4 h of irradiation.

essential to the reaction. In the case of adding $K_2Cr_2O_7$, a low amount of gas products was detected without CH_3OH, suggesting that reduction of e^- is adverse to generation of CH_3OH. These data indicated that the active species enhance the reaction in the order of •OH > e^- > h^+.

The aforementioned PL spectra, transient photocurrent response, and EIS characterizations confirm the formation of photogenerated carriers from composite Cu/ZnV_2O_4, as shown in eqs 1 and 2.

$$ZnV_2O_4 \rightarrow ZnV_2O_4(h^+) + ZnV_2O_4(e^-) \quad (1)$$

$$Cu + e^- \rightarrow Cu(e^-) \quad (2)$$

The calculated CB position for ZnV_2O_4 (−0.44 eV) is lower than the reduction reaction potential of $E(CO_2/CH_3OH)$ = −0.38 eV, $E(CO_2/C_2H_5OH)$ = −0.35 eV, and $E(CO_2/CH_4)$ = −0.25 eV. The VB position of ZnV_2O_4 (2.51 eV) is higher than the oxidation reaction potential of $E(H_2O/{}^\bullet OH)$ = 2.31 eV, theoretically matching the redox requirement of CO_2 or H_2O.

Under UV−vis light irradiation, electrons transit from VB to CB, and the Cu-ZnV_2O_4 heterojunction interface promotes electron transport. Some excited electrons of high energy migrate through the Schottky barrier to the Cu surface and react with CO_2 to generate the products. The energy band bending induces generation of CO ($E(CO_2/CO)$ = −0.52 eV). The occurrence of the photocatalytic reaction was proposed as shown in Figure 15.

https://doi.org/10.1021/acsomega.1c07108
ACS Omega 2022, 7, 7278−7286

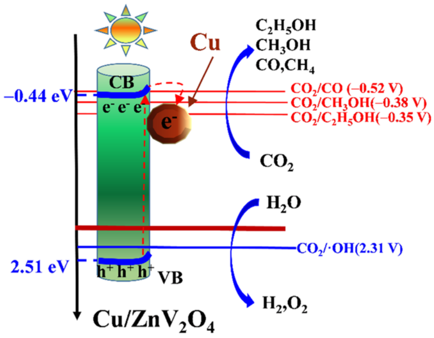

Figure 15. Electron transfer and photoreaction on Cu-ZnV_2O_4.

The electrons (e^-) in the CB of ZnV_2O_4 migrate to the Cu interface, reducing CO_2 aerated H_2O to CO, CH_3OH, CH_4, and C_2H_5OH.

The holes (h^+) left in the VB of ZnV_2O_4 promote oxidation of H_2O. The produced $^\bullet$OH and H^+ participate in the CO_2 reduction, as shown in eqs 3−7.

$$H_2O + h^+ \rightarrow \cdot OH + H^+ \quad (3)$$

$$CO_2 + 2e^- + 2H^+ \rightarrow CO + H_2O \quad (4)$$

$$CO_2 + 6e^- + 6H^+ \rightarrow CH_3OH + H_2O \quad (5)$$

$$2CO_2 + 12e^- + 12H^+ \rightarrow C_2H_5OH + 3H_2O \quad (6)$$

$$CO_2 + 8e^- + 8H^+ \rightarrow CH_4 + 2H_2O \quad (7)$$

■ CONCLUSIONS

For photogeneration of methanol and ethanol from CO_2 and H_2O, composite metal−semiconductor Cu/ZnV_2O_4 heterojunction nanorods were successfully synthesized by a two-step hydrothermal reduction method. Cu^0-ZnV_2O_4 improves the visible light harvest and surface area and results in a faster transport of photogenerated electrons, which can be tuned through varying the composite amount of Cu_2O. The energy band position of the Cu^0-ZnV_2O_4 heterojunction matches with the photoreaction to methanol and ethanol. Cu^0 on the surface of ZnV_2O_4 not only increases the active sites but also accelerates electron transfer in the Cu^0-ZnV_2O_4 heterojunction interface. An increased number of effective photogenerated electrons promotes multielectron reactions for methanol and ethanol generation. With 10Cu/ZnV_2O_4, the total carbon yield for the photocatalytic reduction of CO_2 aerated H_2O was 25.96 μmol·g^{-1} under UV−vis light irradiation for 4 h. The selectivity of CH_3OH and C_2H_5OH reached 50.85 and 13.25%, respectively. 2.5Cu/ZnV_2O_4 showed the highest ethanol yield of 1.58 μmol·g^{-1}·h^{-1}. The promotion is affected by the Cu amount and the UV−vis light response. $^\bullet$OH and e^- were proved to be active intermediate species during the formation of methanol and ethanol. This provides new insights into the heterojunction interface in Cu/ZnV_2O_4 for CO_2 photoreduction in H_2O to methanol and ethanol.

■ EXPERIMENTAL SECTION

Catalyst Preparation. Cu_2O was prepared using hydrothermal reduction in a N_2 atmosphere. Briefly, 0.2 g of $Cu(CH_3COO)_2 \cdot H_2O$ was dissolved in 60 mL of deionized water in a three-neck flask under stirring for 30 min. Then, 0.87 g of sodium dodecyl dimethyl sulfate was added, and the solution was continuously stirred for 20 min. Next, 2.6 mL of NaOH solution (1 M) and 24 mL of $NH_2OH \cdot HCl$ (0.1 M) were added rapidly and stirred vigorously for 1 h. The product was washed with deionized water to adjust the pH to 7 and dried at 80 °C in vacuum for 12 h. Brick-red Cu_2O powder was obtained.

ZnV_2O_4 was synthesized using a solvothermal procedure. Briefly, 0.002 mol of NH_4VO_3 and 0.006 mol of $H_2C_2O_4 \cdot 2H_2O$ were dissolved in 40 mL of *N*,*N*-dimethylformamide and stirred for 30 min. Then, 0.001 mol of $Zn(CH_3COO)_2 \cdot 2H_2O$ was added and continuously stirred for 30 min. The mixture was transferred to an 80 mL Teflon-lined autoclave, heated at 180 °C for 24 h, and then cooled to room temperature. The product was washed with deionized water and ethanol, dried at 80 °C in vacuum for 12 h, and calcined at 550 °C for 5 h. Black ZnV_2O_4 powder was obtained.

For Cu/ZnV_2O_4 preparation, Cu_2O with the desired amount was dispersed in 40 mL of *N*,*N*-dimethylformamide, and the other steps were the same as those for the synthesis of ZnV_2O_4. The composite content of Cu_2O was 1.25, 2.5, 5, 10, and 20 wt % of ZnV_2O_4, and the resulting samples were denoted as 1.25, 2.5, 5, 10, and 20Cu/ZnV_2O_4, respectively.

Characterization. The phase analysis was carried out on a D8 ADVANCE A25 with Cu Kα (λ = 0.1542 nm) at 40 kV/40 mA. Surface area and pore distribution were determined using N_2 adsorption on a JWBK132F instrument. The pore distribution was calculated using the BJH model. Microscopic morphology was observed on a Zeiss Merlin Compact scanning electron microscope at 520 kV using gold sputtering samples or a Talos F200i FETEM at 200 kV using ethanol-dispersed samples. Surface species were analyzed on a Thermo Scientific photoelectron spectrometer with Al Kα and C 1s (284.6 eV) correction. The photoluminescence spectra were recorded on an Edinburgh FLS1000 at an excitation wavelength of 325 nm.

The diffuse reflectance absorption spectra were recorded on a Shimadzu UV-3600 UV−vis−NIR spectrophotometer. The band gap energy (E_g) was calculated according to the Kubelka−Munk equation $(\alpha h\nu)^{1/n} = A(h\nu - E_g)$, where α is the absorption coefficient and n = 1/2 for Cu/ZnV_2O_4. Specifically, E_g was obtained from the intersection of the tangent of the starting curve with the hν axis.[20]

The transient photocurrent response and electrochemical impedance spectroscopy (EIS) were measured on a CHI 760E electrochemical workstation. Working electrode: 3 mg of the sample was placed in a centrifuge tube, and then 200 μL of ethanol and 10 μL of 0.5% Nafen solution were added and ultrasonically dispersed for 1 h. Ag/AgCl was used as the reference electrode. A Pt electrode was the counter electrode, and 0.5 mol/L Na_2SO_4 was the electrolyte solution.

Photocatalytic Reduction Activity Test. A reactor of 100 mL was used with a quartz window and a 300 W UV−vis xenon lamp on the top using a current of 15 A as shown in Figure 16.

Briefly, 40 mg of catalyst and 40 mL of an aqueous solution of NaOH (0.1 M) and Na_2SO_3 (0.1 M) were added to the reactor. The reactor was replaced by CO_2 three times, switched to CO_2 (20 mL/min) for 0.5 h, and then pressed to 0.2 MPa. Photoreduction proceeded under irradiation for set reaction times.

Gas products were analyzed on a GC9560 gas chromatograph with a 5A molecular sieve column (3 m × 3 mm). Liquid products were analyzed on another GC9560 with an FFAP

https://doi.org/10.1021/acsomega.1c07108
ACS Omega 2022, 7, 7278−7286

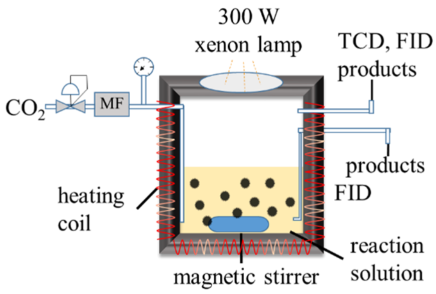

Figure 16. Schematic of the photoreactor for CO_2 and H_2O.

column (30 m × 0.25 mm × 0.25 μm). The qualitative analysis of methanol and ethanol in the liquid products was performed using GC−MS spectra (Figure S1). The results were calculated as Y_i (yield, $\mu mol \cdot g^{-1} \cdot h^{-1}$) = $n_i/m/t$, where n_i, m, and t are product amount (μmol), catalyst mass (g), and reaction time (h), respectively. TC (total carbon yield, $\mu mol \cdot g^{-1} \cdot h^{-1}$) = $Y_{CO} + Y_{CH_4} + Y_{CH_3OH} + Y_{C_2H_5OH}$. S_i (product selectivity, %) = $(Y_i/TC) \times 100$.

■ ASSOCIATED CONTENT

Supporting Information

The Supporting Information is available free of charge at https://pubs.acs.org/doi/10.1021/acsomega.1c07108.

GC−MS spectra for liquid products; photocatalytic activity comparison under UV−vis and visible light irradiation; and XPS spectra for surface elements of synthesized samples (PDF)

■ AUTHOR INFORMATION

Corresponding Author

Tian-Sheng Zhao − *State Key Laboratory of High-efficiency Utilization of Coal and Green Chemical Engineering, College of Chemistry & Chemical Engineering, Ningxia University, Yinchuan 750021, China*; orcid.org/0000-0002-2292-3194; Email: zhaots@nxu.edu.cn

Authors

Huihui Du − *State Key Laboratory of High-efficiency Utilization of Coal and Green Chemical Engineering, College of Chemistry & Chemical Engineering, Ningxia University, Yinchuan 750021, China*

Qingxiang Ma − *State Key Laboratory of High-efficiency Utilization of Coal and Green Chemical Engineering, College of Chemistry & Chemical Engineering, Ningxia University, Yinchuan 750021, China*

Xinhua Gao − *State Key Laboratory of High-efficiency Utilization of Coal and Green Chemical Engineering, College of Chemistry & Chemical Engineering, Ningxia University, Yinchuan 750021, China*; orcid.org/0000-0003-1368-1901

Complete contact information is available at: https://pubs.acs.org/10.1021/acsomega.1c07108

Notes

The authors declare no competing financial interest.

■ ACKNOWLEDGMENTS

The authors acknowledge financial support from the National Natural Science Fund of China (21965028) and the East-West Cooperation Project of Ningxia Key R&D Plan (2017BY063).

■ REFERENCES

(1) Olah, G. Beyond oil and gas: the methanol economy. *Angew. Chem., Int. Ed.* **2005**, *44*, 2636−2639.
(2) Shih, C.; Zhang, T.; Li, J.; Bai, C. Powering the future with liquid sunshine. *Joule* **2018**, *2*, 1925−1949.
(3) Liu, S.-H.; Lu, J.-S.; Pu, Y.-C.; Fan, H.-C. Enhanced photoreduction of CO_2 into methanol by facet-dependent Cu_2O/reduce graphene oxide. *J. CO₂ Util.* **2019**, *33*, 171−178.
(4) Li, X.; Yu, J.; Jaroniec, M.; Chen, X. Cocatalysts for Selective Photoreduction of CO_2 into Solar Fuels. *Chem. Rev.* **2019**, *119*, 3962−4179.
(5) Zhu, L.; Li, H.; Xu, Q.; Xiong, D.; Xia, P. High-efficient separation of photoinduced carriers on double Z-scheme heterojunction for superior photocatalytic CO_2 reduction. *J. Colloid Interface Sci.* **2020**, *564*, 303−312.
(6) Zhang, W.; Mohamed, A.; Ong, W.-J. Z-Scheme Photocatalytic Systems for Carbon Dioxide Reduction: Where Are We Now? *Angew. Chem., Int. Ed.* **2020**, *59*, 22894−22915.
(7) Wang, X.; Wang, Y.; Gao, M.; Shen, J.; Pu, X.; Zhang, Z.; Lin, H.; Wang, X. $BiVO_4/Bi_4Ti_3O_{12}$ heterojunction enabling efficient photocatalytic reduction of CO_2 with H_2O to CH_3OH and CO. *Appl. Catal., B* **2020**, *270*, No. 118876.
(8) Ran, J.; Jaroniec, M.; Qiao, S.-Z. Cocatalysts in Semiconductor-based Photocatalytic CO_2 Reduction Achievements, Challenges, and Opportunities. *Adv. Mater.* **2018**, *30*, No. 1704649.
(9) Duan, F.; Dong, W.; Shi, D.; Chen, M. Template-free synthesis of ZnV_2O_4 hollow spheres and their application for organic dye removal. *Appl. Surf. Sci.* **2011**, *258*, 189−195.
(10) Sajid, M.; Shad, N.; Khan, S.; Zhang, Z.; Amin, N. Facile synthesis of Zinc vanadate $Zn_3(VO_4)_2$ for highly efficient visible light assisted photocatalytic activity. *J. Alloys Compd.* **2019**, *775*, 281−289.
(11) Butt, F.; Cao, C.; Wan, Q.; Li, P.; Idrees, F.; Tahir, M.; Khan, W.; Ali, Z.; Zapata, M.; Safdar, M.; Qu, X. Synthesis, evolution and hydrogen storage properties of ZnV_2O_4 glomerulus nano/microspheres: A prospective material for energy storage. *Int. J. Hydrogen Energy* **2014**, *39*, 7842−7851.
(12) Liu, Y.; Li, C.; Xu, J.; Ou, M.; Fang, C.; Sun, S.; Qiu, Y.; Peng, J.; Lu, G.; Li, Q.; Han, J.; Huang, Y. Electro activation-induced spinel ZnV_2O_4 as a high-performance cathode material for aqueous zinc-ion battery. *Nano Energy* **2020**, *67*, No. 104211.
(13) Bafaqeer, A.; Tahir, M.; Amin, N. Well-designed ZnV_2O_6/g-C_3N_4 2D/2D nanosheets heterojunction with faster charges separation via PCN as mediator towards enhanced photocatalytic reduction of CO_2 to fuels. *Appl. Catal., B* **2019**, *242*, 312−326.
(14) Yan, Y.; Yu, Y.; Wu, D.; Yang, Y.; Cao, Y. TiO_2/vanadate ($Sr_{10}V_6O_{25}$, $Ni_3V_2O_8$, $Zn_2V_2O_7$) heterostructure photocatalysts with enhanced photocatalytic activity for photoreduction of CO_2 into CH_4. *Nanoscale* **2016**, *8*, 949−958.
(15) Tahir, M. Hierarchical 3D VO_2/ZnV_2O_4 microspheres as an excellent visible light photocatalyst for CO_2 reduction to solar fuels. *Appl. Surf. Sci.* **2019**, *467*−*468*, 1170−1180.
(16) Ali, S.; Razzaq, A.; Kim, A.; In, S.-I. Activity, selectivity, and stability of earth-abundant $CuO/Cu_2O/Cu^0$-based photocatalysts toward CO_2 reduction. *Chem. Eng. J.* **2022**, *429*, No. 131579.
(17) Ola, O.; Maroto-Valer, M. Copper based TiO_2 honeycomb monoliths for CO_2 photoreduction. *Catal. Sci. Technol.* **2014**, *4*, 1631−1637.
(18) Wu, Y.; McNulty, I.; Liu, C.; Lau, K.; Liu, Q.; Paulikas, A.; Sun, C.-J.; Cai, Z.; Guest, J.; Ren, Y.; Stamenkovic, V.; Curtiss, L.; Liu, Y.; Rajh, T. Facet-dependent active sites of a single Cu_2O particle photocatalyst for CO_2 reduction to methanol. *Nat. Energy* **2019**, *4*, 957−968.

(19) Luévano-Hipólito, E.; Torres-Martínez, L. Dolomite-supported Cu_2O as heterogeneous photocatalysts for solar fuels production. *Mater. Sci. Semicond. Process.* **2020**, *116*, No. 105119.

(20) Dedong, Z.; Maimaiti, H.; Awati, A.; Yisilamu, G.; Sun, F.; Ming, W. Synthesis and photocatalytic CO_2 reduction performance of Cu_2O/Coal-based carbon nanoparticle composites. *Chem. Phys. Lett.* **2018**, *700*, 27−35.

(21) Li, H.; Lei, Y.; Huang, Y.; Fang, Y.; Xu, Y.; Zhu, L.; Li, X. Photocatalytic reduction of carbon dioxide to methanol by Cu_2O/SiC nanocrystallite under visible light irradiation. *J. Nat. Gas Chem.* **2011**, *20*, 145−150.

(22) Li, H.; Zhang, X.; MacFarlane, D. Carbon Quantum Dots/Cu_2O Heterostructures for Solar-Light-Driven Conversion of CO_2 to Methanol. *Adv. Energy Mater.* **2015**, *5*, No. 1401077.

(23) Ge, H.; Zhang, B.; Liang, H.; Zhang, M.; Fang, K.; Chen, Y.; Qin, Y. Photocatalytic Conversion of CO_2 into Light Olefins over TiO_2 Nanotube confined Cu Clusters with high ratio of Cu^+. *Appl. Catal., B* **2020**, *263*, No. 118133.

(24) Ibarra-Rodríguez, L. I.; Huerta-Flores, A.; Torres-Martinez, L. Development of $Na_2Ti_6O_{13}$/CuO/Cu_2O heterostructures for solar photocatalytic production of low-carbon fuels. *Mater. Res. Bull.* **2020**, *122*, No. 110679.

(25) Zhu, S.; Chen, X.; Li, Z.; Ye, X.; Liu, Y.; Chen, Y.; Yang, L.; Chen, M.; Zhang, D.; Li, G.; Li, H. Cooperation between inside and outside of TiO_2: Lattice Cu^+ accelerates carrier migration to the surface of metal copper for photocatalytic CO_2 reduction. *Appl. Catal., B* **2020**, *264*, No. 118515.

(26) Jiang, Z.; Sun, W.; Miao, W.; Yuan, Z.; Yang, G.; Kong, F.; Yan, T.; Chen, J.; Huang, B.; An, C.; Ozin, G. Living Atomically Dispersed Cu Ultrathin TiO_2 Nanosheet CO_2 Reduction Photocatalyst. *Adv. Sci.* **2019**, *6*, No. 1900289.

(27) Long, R.; Li, Y.; Liu, Y.; Chen, S.; Zheng, X.; Gao, C.; He, C.; Chen, N.; Qi, Z.; Song, L.; Jiang, J.; Zhu, J.; Xiong, Y. Isolation of Cu Atoms in Pd Lattice: Forming Highly Selective Sites for Photocatalytic Conversion of CO_2 to CH_4. *J. Am. Chem. Soc.* **2017**, *139*, 4486−4492.

(28) Xiong, Z.; Xu, Z.; Li, Y.; Dong, L.; Wang, J.; Zhao, J.; Chen, X.; Zhao, Y.; Zhao, H.; Zhang, J. Incorporating highly dispersed and stable Cu^+ into TiO_2 lattice for enhanced photocatalytic CO_2 reduction with water. *Appl. Surf. Sci.* **2020**, *507*, No. 145095.

(29) Li, X.-H.; Antonietti, M. Metal nanoparticles at mesoporous N-doped carbons and carbon nitrides: functional Mott−Schottky heterojunctions for catalysis. *Chem. Soc. Rev.* **2013**, *42*, 6593−6604.

(30) Li, P.; Liu, L.; An, W.; Wang, H.; Guo, H.; Liang, Y.; Cui, W. Ultrathin porous g-C_3N_4 nanosheets modified with AuCu alloy nanoparticles and C-C coupling photothermal catalytic reduction of CO to ethanol. *Appl. Catal., B* **2020**, *266*, No. 118618.

(31) Fan, Q.; Zhang, X.; Ge, X.; Bai, L.; He, D.; Qu, Y.; Kong, C.; Bi, J.; Ding, D.; Cao, Y.; Duan, X.; Wang, J.; Yang, J.; Wu, Y. Manipulating Cu Nanoparticle Surface Oxidation States Tunes Catalytic Selectivity toward CH_4 or C_2^+ Products in CO_2 Electroreduction. *Adv. Energy Mater.* **2021**, *11*, No. 2170187.

(32) Zhu, Z.; Yang, C.-X.; Hwang, Y.-T.; Lin, Y.-C.; Wu, R.-J. Fuel generation through photoreduction of CO_2 on novel Cu/$BiVO_4$. *Mater. Res. Bull.* **2020**, *130*, No. 110955.

(33) Velu, S.; Suzuki, K.; Gopinath, C. S. Photoemission and in Situ XRD Investigations on CuCoZnAl-Mixed Metal Oxide Catalysts for the Oxidative Steam Reforming of Methanol. *J. Phys. Chem. B* **2002**, *106*, 12737−12746.

(34) Roy, K.; Vinod, C. P.; Gopinath, C. S. Design and Performance Aspects of a Custom-Built Ambient Pressure Photoelectron Spectrometer toward Bridging the Pressure Gap: Oxidation of Cu, Ag, and Au Surfaces at 1 mbar O_2 Pressure. *J. Phys. Chem. C* **2013**, *117*, 4717−4726.

(35) Shiju, N.; Anilkumar, M.; Mirajkar, S.; Gopinath, C.; Rao, B.; Satyanarayana, C. Oxidative dehydrogenation of ethylbenzene over vanadia-alumina catalysts in the presence of nitrous oxide: structure-activity relationship. *J. Catal.* **2005**, *230*, 484−492.

(36) Sivaranjani, K.; Verma, A.; Gopinath, C. S. Molecular oxygen-assisted oxidative dehydrogenation of ethylbenzene to styrene with nanocrystalline $Ti_{1-x}V_xO_2$. *Green Chem.* **2012**, *14*, 461−471.

(37) Ke, X.; Zhang, J.; Dai, K.; Lv, J.; Liang, C. Novel visible-light-driven direct Z-scheme $Zn_3V_2O_8$/Ag_3PO_4 heterojunctions for enhanced photocatalytic performance. *J. Alloys Compd.* **2019**, *799*, 113−123.

(38) Zhang, M.; Cheng, G.; Wei, Y.; Wen, Z.; Chen, R.; Xiong, J.; Li, W.; Han, C.; Li, Z. Cuprous ion (Cu^+) doping induced surface/interface engineering for enhancing the CO_2 photoreduction capability of $W_{18}O_{49}$ nanowires. *J. Colloid Interface Sci.* **2020**, *572*, 306−317.

https://doi.org/10.1021/acsomega.1c07108
ACS Omega 2022, 7, 7278−7286